PCCP

Modulation of methylene blue photochemical properties based on adsorption at aqueous micelle interfaces

Helena C. Junqueira, Divinomar Severino, Luis G. Dias, Marcos S. Gugliotti and Mauricio S. Baptista*

Departamento de Bioquímica, IQ-USP, Av. Prof. Lineu Prestes, 748, São Paulo, SP, Brazil 05513-970. E-mail: baptista@iq.usp.br

Received 25th October 2001, Accepted 12th March 2002
First published as an Advance Article on the web 26th April 2002

Methylene Blue (MB^+) is a sensitizer that has been used for a variety of applications including energy conversion and photodynamic therapy (PDT). Although its photochemical properties in isotropic solution are well established, its effect *in vivo* and in restricted reaction environments is somewhat erratic. In order to understand its photochemical behavior when it interacts with biomolecules, in particular with membranes, MB^+ properties were studied in sodium dodecyl sulfate (SDS) and cetyl trimethylammonium bromide (CTAB) solutions. Because of an electrostatic attraction, SDS and MB^+ form complexes, changing the properties of both the micelles and the MB^+ solutions. Surface tension measurements show that the c.m.c. of SDS decreases from ~7 mM to ~70 μM when the MB^+ concentration increases from 0 to 45 μM. Above the c.m.c., binding of MB^+ in the micelle pseudo-phase causes the formation of aggregates (mostly dimers) as attested by the increase in the absorption at 580 nm and the decrease in fluorescence emission. The extent of dimer formation is dependent on the relative concentrations of MB^+ and SDS. In the presence of excess of SDS, MB^+ is mainly in the monomer form and at low SDS concentration dimers are favored. Such effect, which was not observed in CTAB micelles, was modeled qualitatively by considering that MB^+ molecules partition to the micelle pseudo-phase which favors or disfavors dimers as a function of its volume. MB^+ transient species were characterized by laser flash photolysis and NIR emission showing the presence of triplets and subsequently singlet oxygen at high SDS concentration and semi-reduced and semi-oxidized MB^+ radicals at low SDS concentration. Therefore it was shown that, depending on the ground state MB^+ monomer/dimer equilibrium, induced by the micelles, the photochemical properties of MB^+ can be shifted from a Type II (energy transfer to oxygen forming singlet oxygen) to a Type I mechanism (electron transfer forming the semi-reduced and the semi-oxidized radicals of MB^+).

Introduction

Sensitization processes are extremely important in several areas including biology, chemistry and medicine.[1] Fundamental processes of living organisms such as photosynthesis depend on light absorption and subsequent photophysical and photochemical processes.[2] The application of sensitization to medicine has become extremely important, specially in the new method of cancer treatment known as photodynamic therapy (PDT), where photoinduced *in situ* generation of reactive species has been used to induce tumor regression.[3] In both mentioned cases, processes of energy and/or electron transfer are involved and the knowledge of how these processes are affected/modulated by biological environments (membranes, proteins) is important.[1–4]

The mechanisms of tumoral destruction involve direct oxidation (mechanisms Type I) of biological targets (membranes, proteins and DNA), as well as oxidation mediated by singlet oxygen ($^1O_2$) (mechanisms Type II), which is mainly formed through energy transfer from triplets to molecular oxygen.[5] Binding of molecules in membranes and interfaces can cause several alterations in their ground state properties (dimerization and/or ion-pair equilibria) and consequently in the photophysical and photochemical processes in which they are involved.[6,7] The details of these processes need to be further investigated for the case of sensitizers used in photodynamic therapy, in which the photodynamic effect will happen in cells or tissues, where the photosensitizers will be interacting with macromolecules or membranes.[7,8]

Adsorption of dyes into oppositely charged interfaces, for instance, micelles or polyelectrolytes, has been extensively studied.[9–13] Depending on the charge ratio between the dyes and the charged groups in the colloid interface, dye aggregates are favored.[9,10] This field of dye–surfactant interaction is of great relevance to the dyeing and photography industry.[11] However, there has been little effort towards proposing equilibrium schemes to model dimerization in micelle solution.[10] The effect of the dye on the micellization properties of surfactants has also been studied to a lesser extent.[12,13] Guo and coworkers have used long-chain dyes which themselves act as surfactants. Their results were interpreted in terms of the Lange and Beck theory that proposes an ideal mixture between surfactants. Deviations from ideality were observed when the long-chain dyes and surfactants have opposite charges.[12]

Microheterogeneous systems are known to promote differential distribution of substrates, intermediates and products, in the organic, aqueous or interfacial regions, which can usually be explained by a combination of electrostatic interaction and hydrophobic effect.[1,2,14] Due to these effects, interesting changes in photochemical processes have been observed in micelles, reversed micelles, microemulsions and vesicle systems, including yield enhancements,[14,15] variation of regioselectivity and stereoselectivity,[16,17] change in mechanisms,[18–20] enhanced charge separation,[21,22] magnetic effects[23] and increased

 DOI: 10.1039/b109753a

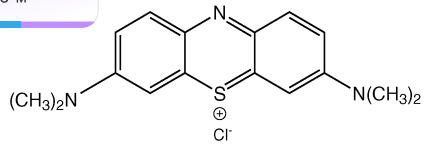

Scheme 1 Molecular structure of Methylene Blue (MB^+).

efficiency of $^1O_2$ generation.[24–28] The literature concerning the effect of solvent[27a,b] and compartmentalization[27c] in $^1O_2$ bimolecular processes is extensive.

The relative importance of Type I and Type II photosensitization reactions and the subsequent damage of biological targets is a recurrent topic in the photochemical literature.[7,8,29–31] It has been shown that the binding of positively charged sensitizers to protein may favor Type I processes because of several factors, including more rigid environment, protection of triplets from oxygen suppression, facilitating protein–sensitizer electron transfer reactions and formation of sensitizer aggregates induced by the protein hydrophobic pockets.[7,8,30,31] Most studies with membranes have emphasized the increase in Type II reactions subsequent to the sensitizer binding in the membrane, due to the decrease in dimerization of the sensitizers (usually porphyrin and phthalocyanine) and the increased oxygen concentration in the less polar media, thereby resulting in an increase in the $^1O_2$ yield.[24–28]

Methylene Blue (MB^+, Scheme 1) is a sensitizer that has been used *in vitro* for a variety of applications including energy conversion and photodynamic therapy. It is especially useful due to the high quantum yield of $^1O_2$ generation ($\phi_\Delta \sim 0.5$),[32] making it valuable for *in vitro* photoxygenation of biological materials or organic precursors.[33–37]

Its photoinduced effect in cell culture or *in vivo* is somewhat erratic.[38–41] There are unexplained reports of MB^+ being inactive photochemically.[38–40] Also the photodynamic efficiency of phenothiazine dyes has been shown to be dependent on the solution pH[40] as well as the octanol/water partition coefficient of the ground state molecule, that changes its affinity to protein, membranes or DNA targets.[41] In general, the photochemical mechanism and efficiency seem to be dependent on the location of the sensitizer, which can alter its ground state and excited state properties.[38–41] In order to mimic its photochemical behavior when it interacts with biological samples, in particular with membranes, MB^+ ground state and excited state properties have been studied in SDS and CTAB solutions. Due mainly to an electrostatic interaction, SDS and MB^+ form complexes that change the properties of both the micelle and the MB^+ solution equilibria. Depending on the surfactant/dye molar ratio MB^+ dimers are favored, and the photochemistry of MB^+ is shifted from a preponderantly singlet oxygen to a mainly radical generator, without addition of any other photoactive or redox agent.

Materials and methods

Materials

MB^+ was acquired from Aldrich and double recrystallized from ethanol. 1,4-Diazabicyclo[2.2.2]octane (DABCO 98%, Aldrich), SDS and CTAB (Merck, 99% HPLC grade) were used without further purification. D_2O (99%) was acquired from Aldrich. Water was bidistilled from an all-glass apparatus and was further purified *via* a Millipore Milli-Q system. All other materials were of the best analytical grade available. All solutions were prepared and used on the same day. To avoid buffer effects in the photochemical behavior the measurements were performed in Milli-Q water.[37] The solution pHs were measured to be within 6.4 ± 0.3.

Instruments and methods

Absorbance spectra were recorded in a Shimadzu UV-2400-PC interfaced to a Pentium II and fluorescence spectra were recorded in a SPEX DM3000-F, using 1 or 0.1 cm optical path length quartz cuvettes. Spectral data were further manipulated with a 386 GRAMS software (Galatic,Inc).

Laser flash photolysis data were obtained with an Applied Photophysics system composed of a Nd:YAG laser (Spectron Laser System, England) operating at 532 nm delivering pulses with ~30 mJ pulse^{-1} and ~10 ns (FWHM) and a pulsed 150 W Xe lamp. Control electronics and a Hewlett Packard 54510B digitizing oscilloscope were used for data capture. For the NIR emission measurements a homemade cell compartment coupled with a germanium PIN detector (EG&Judson, Model J16D-M204-R05M-WB) was used. Transients were stored and analyzed in a 386 PC compatible microcomputer. Decays were fitted to single or double exponentials using the software Origin (Microcal). The $^1O_2$ decay experiments were performed in D_2O to increase the $^1O_2$ lifetime. No changes in fluorescence and absorbance properties of MB^+ as a function of SDS concentration were observed comparing experiments performed in water and in D_2O.

Surface tension measurements were performed by the ring method[42] by using a De Noüy tensiometer (Fisher Scientific Tensiomat, Mode 21 1993). The c.m.c. were determined by using surface tension x ln [SDS] curves. Excess functions were calculated by using eqn. (1).[42] $d\gamma/d\ln c$ is the slope of the curves from Fig. 1, which were obtained for a surfactant concentration varying from 35 to 50 μM for all MB^+ concentrations.

$$\Gamma = \left(\frac{\partial \gamma}{\partial \ln c}\right)_T \left(-\frac{1}{RT}\right) \quad (1)$$

The concentrations of dimers and monomers were calculated by minimizing the error quadratic function (eqn. (2)) between the measured MB^+ absorbance spectra in SDS solutions ($A_{exp}(i)$) with the absorbance spectra of the monomer and dimer ($A_{calc}(i)$).

$$E = \sum_{i=\lambda_{min}}^{\lambda_{max}} (A_{exp}(i) - A_{calc}(i))^2 \quad (2)$$

The calculated absorbance spectra were obtained by using the absorbance spectra of monomers and dimers (eqn. (3)) and the mass balance equation (eqn. (4)).

$$A_{calc}(i) = \varepsilon_M(i) l_M [M] + \varepsilon_D(i) l_D [D] \quad (3)$$

$$[M] + 2[D] = C_T = \frac{C_T - [M]}{2} \quad (4)$$

where $\varepsilon_M(i)$ and $\varepsilon_D(i)$ are the absorbance spectra of monomers and dimers, respectively in molar extinction coefficient units, l is the cuvette path length (1 cm), [M] and [D] are the monomer and dimer equilibrium concentrations and C_T is the total MB^+ concentration. The monomer and dimer absorbance spectra were obtained from the literature.[43,44]

Results and discussion

Effect of MB^+ on the SDS solution and interfacial properties

Aqueous SDS micelles are dynamic entities, in which the micelle structure is in equilibrium with solution monomers and the surfactant monolayer at the air/water interface.[45] MB^+ is positively charged having therefore a strong attraction for SDS. This interaction is likely to change the solution equilibrium of SDS. In order to investigate in detail the effect of MB^+ in the micelle properties of SDS, surface tension (γ) measurements as a function of SDS concentration for several concentrations of MB^+ were performed (Fig. 1). The c.m.c. is

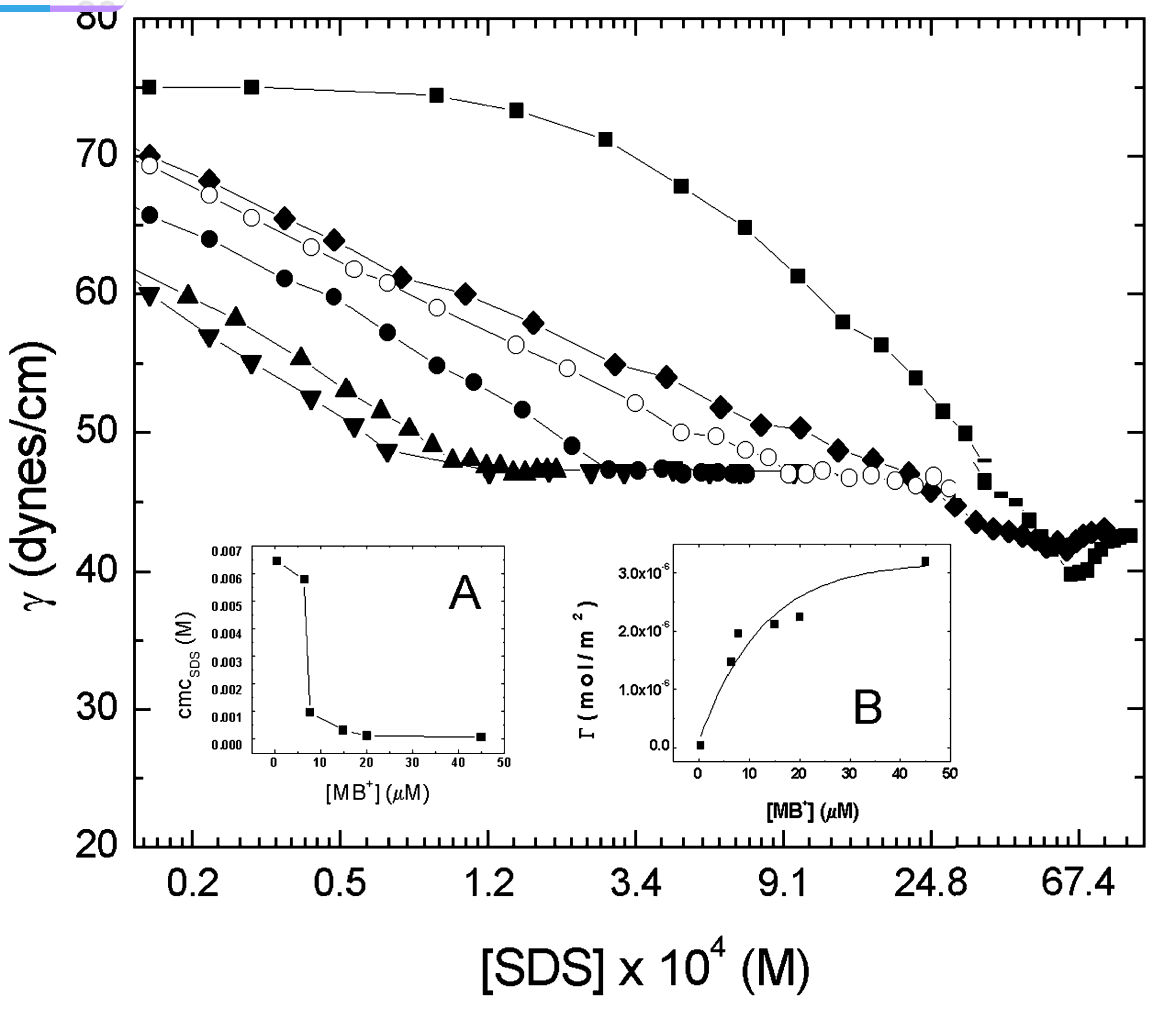

Fig. 1 Surface tension (γ) as a function of SDS concentration at different MB^+ concentrations (in μM): 0.5 (■) 5 (◆) 7.7 (○) 15 (●) 20 (▲) 45 (▼). Inset A: critical micelle concentration (c.m.c.) of SDS as a function of MB^+ concentration. Inset B: excess function of SDS (Γ) as a function of MB^+ concentration.

reached at lower SDS concentrations (Fig. 1, Inset A) as the MB^+ concentration is increased. In fact, the c.m.c. of SDS decreases from ~7 mM to ~70 μM when the MB^+ concentration increases from 0 to 45 μM. That is to say that the MB^+ facilitates micelle formation.

Salts (common electrolytes) are known to decrease the electrostatic repulsion among monomers in the micelle interface and consequently to decrease the c.m.c.[45] However their effects are observed only at high solute concentration (mM). In the case of MB^+, micromolar concentrations are enough to change the c.m.c. by two orders of magnitude. This effect must be due to a strong interaction between MB^+ and SDS forming complexes that have a higher tendency to stay at the interface (less repulsion among monomers, and lower water solubility). If that is the case, the number of molecules of SDS per surface area (excess function) should increase with the increase in the MB^+ concentration. In fact the excess function increases with the MB^+ concentration (measurements performed from 35 to 50 μM SDS) in a hyperbolic way, suggesting that a SDS/MB^+ binding equilibrium is involved in increasing stability of SDS in the interface (Fig. 1, Inset B).

These experiments attest to the complexity of the multiple equilibria involved in SDS/MB^+ solutions. Nevertheless if the SDS concentration is larger than the c.m.c. (5–10 times) one can interpret the results as the MB^+ interacting with micelles. The knowledge gained studying the physical-chemistry properties of SDS/MB^+ solutions can now be used to interpret the photophysical and photochemical results.

Effect of SDS on the MB^+ solution equilibria

MB^+ monomers and dimers have been characterized before and they have distinct absorbance spectra.[43,44] As can be observed in Fig. 2, monomers have a maximum at 665 nm and dimers at 580 nm. Note that by changing the SDS concentration the MB^+ absorbance spectra changes considerably. At low SDS concentration (1 mM) there is an increase in the absorption intensity at around 580 nm, while at high SDS concentration (50 mM), an increase at 665 nm is observed and the spectrum is almost the same as that of pure MB^+ monomer. The difference in absorption between monomers and dimers facilitates the calculation of the concentration of each species present in solution. Furthermore, the ratio of the absorbance at 580 and 665 nm (A_{580}/A_{665}) gives a qualitative estimate of the relative concentration of dimers to monomers.

The absorption spectra of an 8 μM MB^+ solution was measured as a function of SDS and CTAB concentrations and the A_{580}/A_{665} values were calculated. (Fig. 3) It can be noticed that A_{580}/A_{665} increases as a function of SDS concentration up to ~3 mM and then starts to decrease. The increase in A_{580}/A_{665} indicates the increase in the concentration of dimers in relation to monomers. The dimer formation can also be verified by measuring the fluorescence intensity (Fig. 3, Inset). As the A_{580}/A_{665} increases the emission intensity divided by the fraction of light absorbed at the excitation wavelength (I_F/f_{580}) decreases, indicating the presence of dimers, probably H type dimers, which are not fluorescent and have an increased

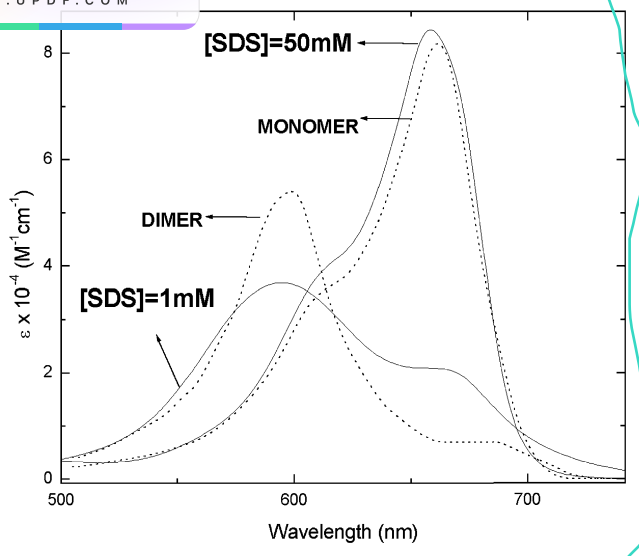

Fig. 2 MB^+ absorption spectra at 1.0 and 50 mM SDS concentrations (continuous line, $[MB^+] = 30$ μM) and monomer and dimer absorbance spectra[43,44] (dashed line).

absorption in the blue region of the spectra.[43,44] Below the c.m.c. there are variations in both A_{580}/A_{665} and I_F/f_{580}, indicating the possible presence of pre-micellar aggregates, which could also alter the monomer/dimer MB^+ equilibrium. At high surfactant concentration (20–30 × c.m.c.), practically all MB^+ molecules are bound to the micelles. Because there is a large excess of micelles in relation to MB^+ molecules, dimers are disfavored by the distribution of monomers through different micelles. At intermediate concentrations (~5–10 × c.m.c.), MB^+ molecules are also strongly attracted to the micelles. Because of the small volume of the micelle pseudo-phase under these conditions, higher "local" MB^+ concentration is induced, and dimer formation is maximized. It is important to notice that the MB^+ dimer equilibrium constant was calculated to be 3.8×10^3 M^{-1} in water, which is accordance with other published results.[43,44] Therefore, at 8 μM only 2% MB^+ are expected in the dimer form in aqueous solutions, compared with 70–80% of dimers that are observed at certain micelle concentrations.

In order to modulate the effect of micelles on the dimerization equilibria of MB^+, a phenomenological model was applied which is aimed to predict qualitatively the variation of monomer and dimer concentrations as a function of detergent concentration (Scheme 2). Because small MB^+ concentrations are used (micromolar range), the dimerization constant in the aqueous phase was ignored. The equations that describe these equilibria are the mass balance (eqn. (5)), the relation between the "local" micelle concentration and the analytical concentration of each of the species involved (eqn. (6)), the partition equilibrium constant (eqn. (7)) and the dimerization constant in the micelle phase (eqn. (8)). Note that the partition constant is defined as the ratio of the total MB^+ concentration in the micelle pseudo-phase ($[M^M] + 2[D^M]$) divided by the total concentration of MB^+ in the aqueous phase, which is assumed to be equal to $[M^W]$.

$$C_T = [M^W] + [M^M] + 2[D^M] \quad (5)$$

where C_T is the total MB^+ concentration, the superscripts M and W indicate the micelle pseudo-phase and aqueous phases, respectively.

$$[X_{micelle}] = \frac{[X_{analytical}]}{C_D V} \quad (5)$$

Where $[X_{analytical}]$ is the concentration of X calculated by absorption measurements using eqn. (1) and eqn. (2), $[X_{micelle}]$

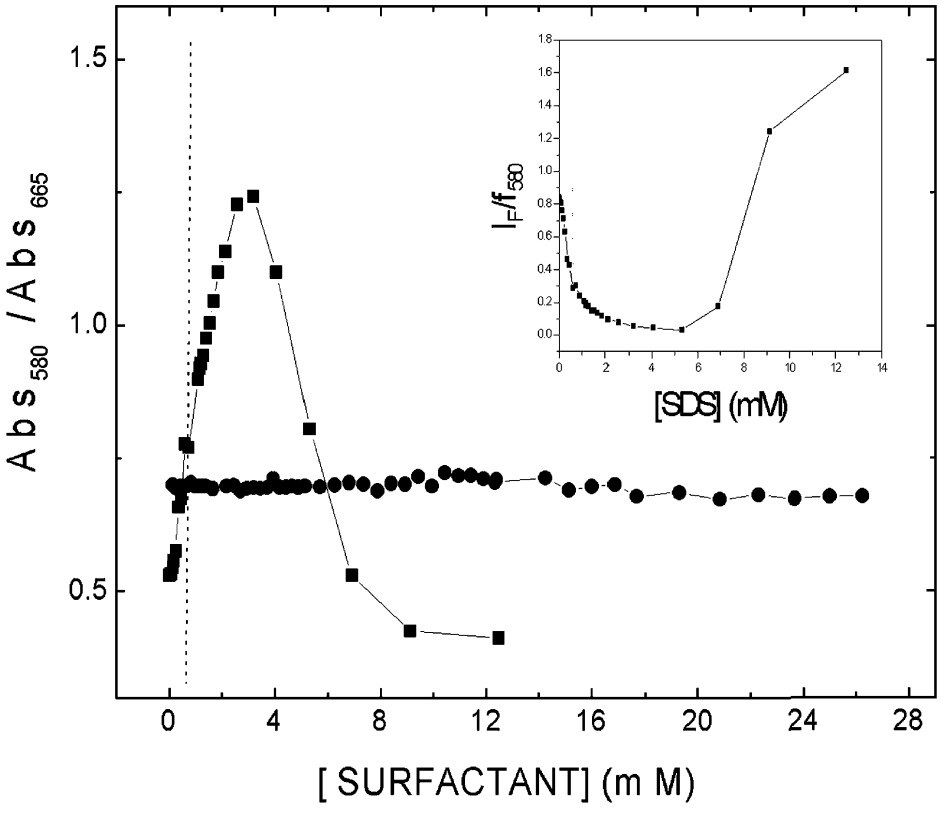

Fig. 3 Ratio of the absorbance value at 580 and 665 nm (A_{580}/A_{665}) of MB^+ as a function of SDS (■) and CTAB (●) concentrations. Inset: Integrated fluorescence intensity (590–750 nm, $\lambda_{exc} = 580$ nm) divided by the fraction of absorbed light at the excitation wavelength (I_F/f_{580}) as a function of SDS concentration. The dashed lines represent the SDS c.m.c. value at this MB^+ concentration (c.m.c. = 0.96 mM), $[MB^+] = 8$ μM.

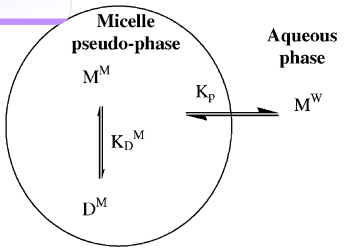

Scheme 2 Pseudo-phase model for the binding and dimerization of dye molecules in micelle solutions. M and D represent monomer and dimer dye molecules, superscript M and W represent micelle and aqueous pseudo-phases, K_P is the partition constant, and K_D the dimerization constant.

is the local concentration in the micelle pseudo-phase, C_D is the concentration of micellized surfactant ([SDS]-c.m.c.), and V is the micelle molar volume (0.39 M^{-1} for SDS).[46]

$$K_P = \frac{([M^M] + 2[D^M])/C_D V}{[M^W]} \quad (7)$$

$$K_D{}^M = \frac{[D^M]/C_D V}{([M^M]/C_D V)^2} = \frac{[D^M]C_D V}{[M^M]^2} \quad (8)$$

At SDS concentrations at which the A_{580}/A_{665} curve has a decreasing trend ([SDS] = 3–10 mM, Fig. 3 and Fig. 4 lower panel), the ratio of SDS to MB^+ concentration is around 10^2–10^3. Considering the strong MB^+/SDS interaction, it can be assumed that in this condition all the MB^+ molecules are in the micelle pseudo-phase, consequently, the monomer and dimer concentrations obtained from the absorbance spectra are their respective concentrations in the micelle pseudo-phase. According to eqn. (8) by plotting $[D^M]/[M^M]^2$ as a function of the inverse of the micelle pseudo-phase volume ($1/(C_D V)$) a straight line is expected whose slope is $K_D{}^M$ (Fig. 4A). $K_D{}^M$ was calculated to be 295 M^{-1}, which is 10 times smaller than the dimerization in water ($K_D = 3.8 \times 10^3$ M^{-1}). The energetics of dimerization of dye molecules has an important hydrophobic component.[9–13] The decrease in K_D is probably the result of the smaller hydrophobic interaction between dye molecules in the micelle environment compared with the hydrophobic interaction in water. Therefore, within this model, the increase in dimer concentration in micelle solution is explained solely by the much smaller volume of the micelle pseudo-phase at small SDS concentrations.

Using this value of the dimerization constant as well as the absorbance data it is possible to calculate the partition constant. In the ascending part of the A_{580}/A_{665} curve (Fig. 4 lower panel) the monomer concentration extracted from the absor-

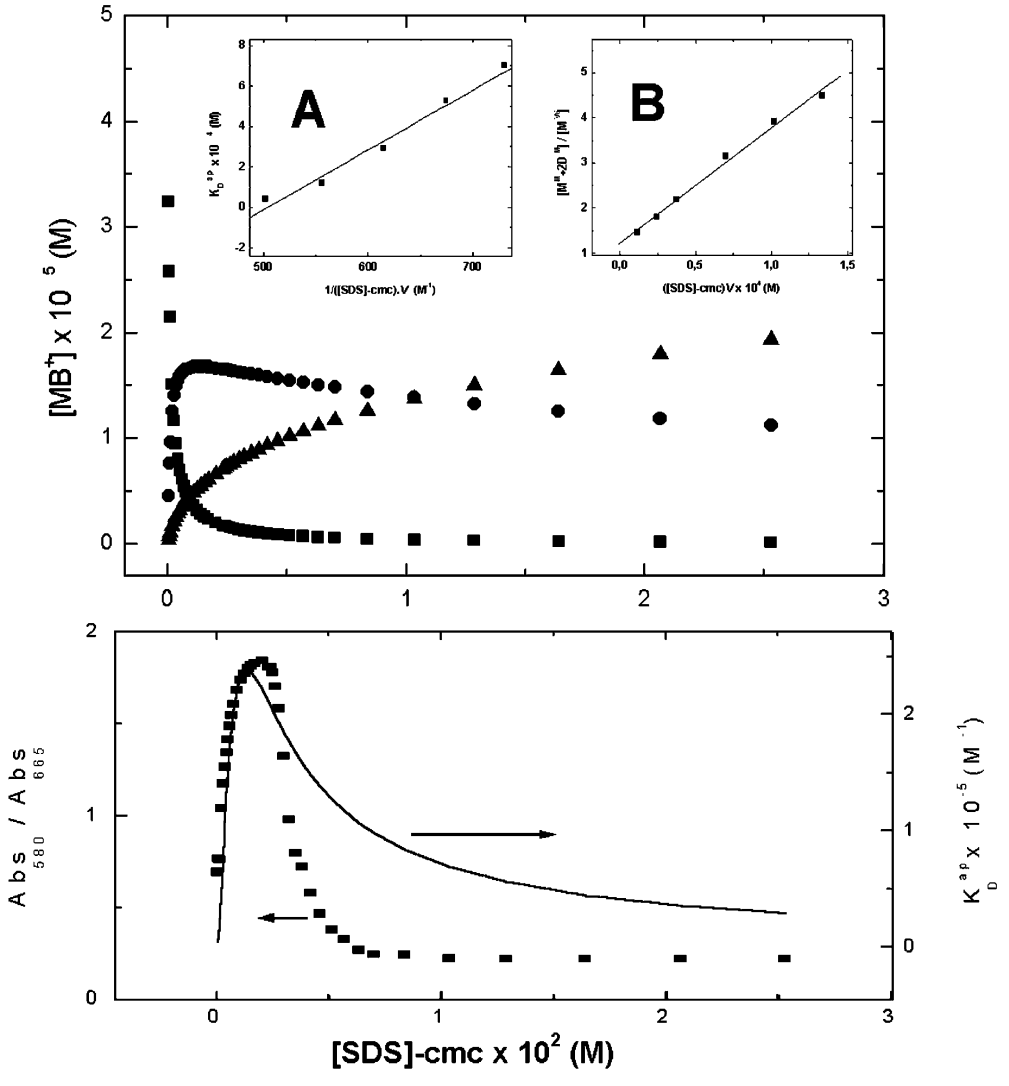

Fig. 4 Upper panel: Concentrations of dimers in micelles, $[D^M]$ (●), monomers in water, $[M^W]$ (■), monomers in micelles, $[M^M]$ (▲) as a function of micellized SDS (C_D = [SDS]-c.m.c.). $[D^M]$, $[M^W]$ and $[M^M]$ were obtained by solving eqns. (7) and (8). Inset A: Plot of $K_D{}^{app}$as a function of $1/C_D V$, Inset B: Plot of $([M^M] + 2[D^M])/[M^W]$ as a function of $C_D V$. Lower panel: (■) A_{580}/A_{665} as a function of micellized SDS concentration, and $K_D{}^{app}$ as a function of micellized SDS (continuous line).

bance spectra comes from monomers in the micelle pseudo-phase as well as from monomers in the aqueous phase. The concentration of monomers in the micelle pseudo-phase can be calculated using the dimer concentration (extracted directly from the absorbance spectra) and the calculated dimerization constant ($K_D^M = 295\ M^{-1}$). Therefore, it is possible to calculate the concentrations of all the species involved in this equilibrium ($[M^W]$, $[M^M]$, $[D^M]$). By plotting $([M^M]+2[D^M])/[M^W]$ as a function of $C_D V$ (Fig. 4B), the partition constant was calculated to be $2.5\times10^4\ M^{-1}$, which is compatible with the strong SDS/MB^+ interaction. Using these values of the equilibrium constants, the concentrations of M^W, M^M and D^M were calculated as a function of the micellized SDS concentration (Fig. 4 upper panel). It can be observed that at low SDS concentration the model predicts a decrease in the M^W concentration with a consecutive increase in the M^M and D^M concentrations as the SDS concentration increases. While the $[M^M]$ increase follows a hyperbolic curve, $[D^M]$ reaches a maximum and starts to decrease as observed experimentally. Based on these concentrations the value of the apparent dimerization constant ($K_D^{ap} = [D^M]/([M^W]+[M^M])^2$) was calculated as a function of SDS concentration. It can be observed that this function also predicts a maximum in the dimerization constant as observed in the experimentally measured A_{580}/A_{665} curve (Fig. 4, lower panel). It can also be noticed that the absorbance data suggest a higher decrease in the dimer concentration as the SDS concentration increases than that predicted by the model. The reasons for the lack of agreement at high SDS concentrations may be the presence of higher order aggregates in the maximum of the dimer concentration region, which are not considered in the present model.

Modulation of the MB^+ photochemical properties by binding to negatively charged micelles

MB^+ has been extensively used for photo-oxidation of natural and synthetic molecules. Two major photochemical pathways are usually observed:[29,33–41,47–52] Type II where the triplet energy is transferred to oxygen forming singlet oxygen ($^1O_2$) and Type I where reducing agents donate an electron to MB^+ triplets, forming the semi-reduced radical ($MB^{\bullet}$). At high dye concentration, ground state MB^+ molecules can themselves act as reducing agents ($D-{}^3D^*$ mechanism).[47] In homogeneous solution where no dimers are present (in ethanol, for instance) MB^+ produces triplets with high quantum yield ($\phi_T = 0.52$). In the conditions employed in this work, *i.e.*, relatively small dye concentration, in the presence of oxygen and in the absence of reducing agents basically only type II reactions are observed, *i.e.*, MB^+ works as an efficient $^1O_2$ photogenerator ($\phi_\Delta \sim 0.5$).[29,33,34,51,52] In the presence of SDS above the c.m.c., MB^+ binds to the micelle and, depending on the ratio of micelle to MB^+ concentrations, MB^+ aggregates are observed. The photochemical properties of MB^+ can then be modulated by binding to the micelle pseudo-phase.

The photochemical intermediates following laser pulse excitation (Nd:YAG) at 532 nm were monitored by laser flash photolysis. In the presence of excess of micelles (50 mM of SDS) only monomers are present (Fig. 2). It can be noticed that the transient spectrum obtained at this condition has a maximum around 420 nm (Fig. 5A). This transient has been characterized before and is due to MB^+ triplets.[49–51] It has a lifetime of around 1.5 μs (Fig. 5A, Inset), which is the same as the bleaching recovery time measured at 630 nm (Fig. 5A, Inset). These results obtained in excess SDS micelles are compatible with the main deactivation process of MB^+ triplets being controlled by diffusional collision with oxygen (air-saturated) forming $^1O_2$ (reaction (2), Scheme 3, see Fig. 7 for results concerning $^1O_2$ sensitization). Therefore in SDS micelles in the presence of oxygen, MB^+ has a photochemical behavior similar to that observed in isotropic solution, *i.e.*, it is an efficient triplet and singlet oxygen generator.

The transient spectrum (Fig. 5B) of the MB^+ solution in the presence of 1 mM of SDS (80% of dimers are present), is completely different from that observed in the presence of 50 mM

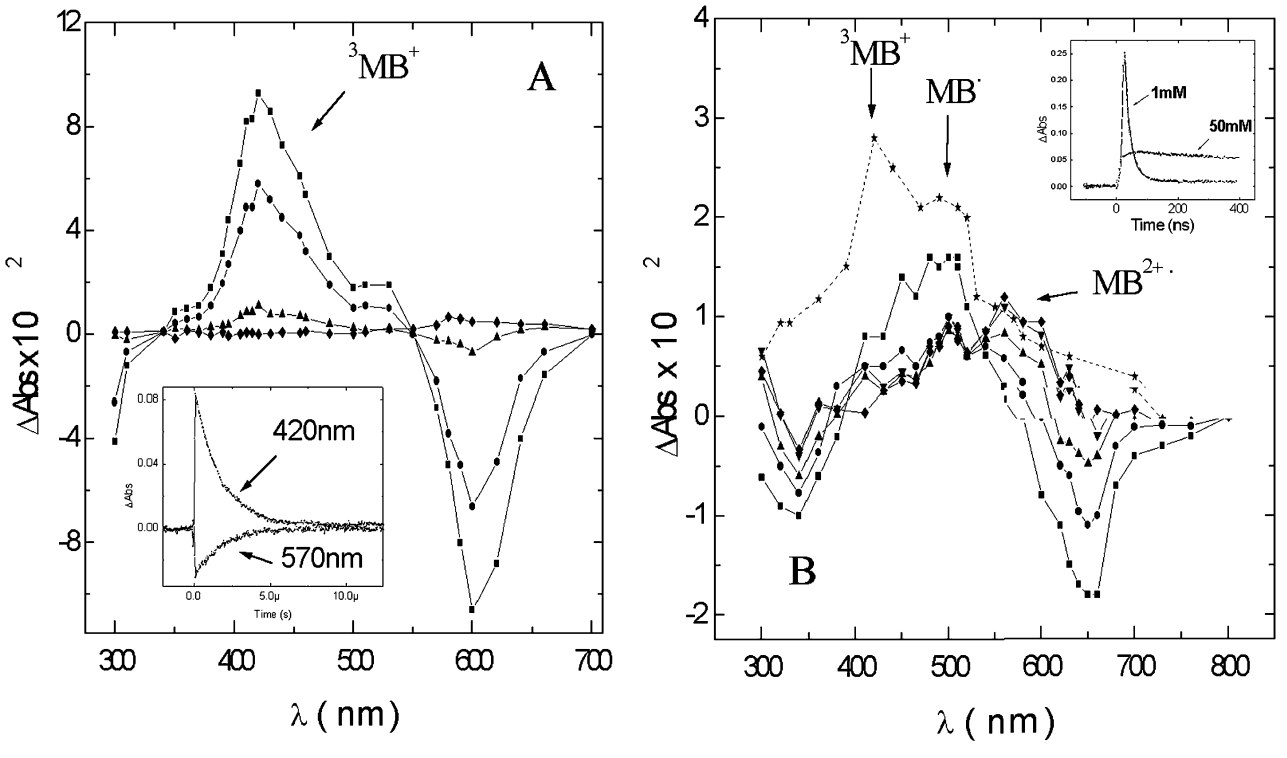

Fig. 5 ΔA of MB^+ solutions containing 50 (A) and 1 (B) mM of SDS measured at 0.1 (■), 1 (●), 4 (▲), 14 (◆) μs after the laser pulse in A and 0.035 (★), 0.15(■), 1 (●), 2 (▲), 7 (▼), 15 (◆) μs after the laser pulse in B. The spectrum in B obtained 35 ns after the laser pulse (★) was scaled down by a factor of 5 in order to fit into the same figure. Excitation at 532 nm, 15 mJ $pulse^{-1}$. Inset A: ΔA as a function of time measured at 420 and 570 nm $[MB^+] = 30$ μM, $[SDS] = 50$ mM. Inset B: ΔA transients measured at 420 nm on the nanosecond time scale in the presence of 1 and 50 mM SDS, $[MB^+] = 30$ μM.

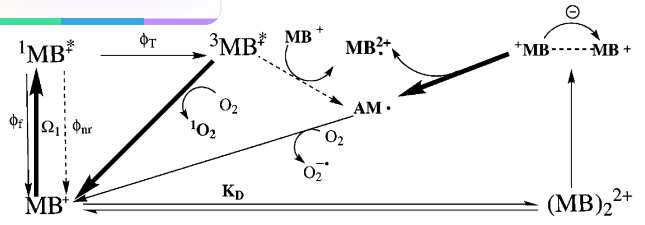

$$^3MB^{+*} \xrightarrow{k_1} MB^+ \quad (1)$$

$$^3MB^{+*} + O_2 \xrightarrow{k_2} MB^+ + {}^1O_2 \quad (2)$$

$$(MB)_2^{2+} \xrightarrow{h\nu} (^3MB^+ \cdots MB^+)^* \xrightarrow{k_3} MB^{\bullet} + MB^{2+\bullet} \quad (3)$$

$$MB^{\bullet} + O_2 \xrightarrow{k_4} O_2^{-\bullet} + MB^+ \quad (4)$$

$$MB^+ + MB^+ \underset{}{\overset{K_D}{\rightleftharpoons}} (MB)_2^{2+} \quad (5)$$

Scheme 3 Methylene Blue photochemical reaction routes where MB^+, $^1MB^{+*}$, $^3MB^{+*}$ are methylene blue ground state, singlet and triplet excited states, respectively, $MB^{\bullet}$ and $MB^{2+\bullet}$ are methylene blue semi-reduced and semi-oxidized radicals, respectively, Ω_1 is light absorption, ϕ_f, ϕ_{nr}, ϕ_T, are fluorescence, nonradiative and triplet quantum yields. Reactions (1)–(4) represent the deactivation routes of MB^+ excited state and radical species where (1) is the $^3MB^{+*}$ spontaneous decay, (2) is the reaction of $^3MB^{+*}$ with molecular oxygen, (3) is the redox suppression of $(^3MB^+\cdots MB)^*$ after excitation of ground state dimers, (4) is the oxidation of $MB^{\bullet}$ by molecular oxygen returning to the ground state dye and forming superoxide, (5) is the ground state dimerization. The relative position of the excited species presented in this scheme, does not represent their actual energy level.

of SDS (Fig. 5A). A few nanoseconds after the laser pulse, the presence of MB^+ triplets ($\Delta A_{max} = 420$ nm) and the semi-reduced radical ($MB^{\bullet}$, $\Delta A_{max} = 530$ nm) is noticed.[49–51] The absorption due to the triplet disappears on the nanosecond time scale ($\tau \sim 40$ ns) (Fig. 5B, Inset), which is much faster than the lifetime measured in excess SDS (Fig. 5A, Inset). At 200 ns after the pulse only $MB^{\bullet}$ species are observed (Fig. 5B). There may be two sources of $MB^{\bullet}$ species, *i.e.*, from singlet or triplet states after the ground state dimer is excited. In our experiment basically only ground state dimers are being excited (at 532 nm, ε of the dimer is 3 times as high as that of the monomer and the dimers are in excess 4 to 1). Considering the intense ΔA measured at 420 nm, which is due to triplets, and the fact that the exciton coupling theory predicts that dimers could have increased intersystem crossing,[53] it is likely that the main mechanism of electron transfer is the dye–dye mechanism through triplets,[47] *i.e.*, reaction (3) of Scheme 3. The transient spectra of $^3MB^+$ observed after exciting ground state monomers or dimers are not distinguishable, at least in our instrumental time resolution (tenths of a nanosecond). This effect may be the result of dimer dissociation in the excited state, although it needs further investigation. $MB^{\bullet}$ decays with a lifetime of ~1.6 μs, which is also compatible with a deactivation mechanism by oxygen forming the anion superoxide (reaction (4), Scheme 3).

Further evidence for this mechanism can be obtained by performing the experiment in the absence of oxygen. It is possible to observe that the fast transient at 420 nm is independent of oxygen concentration, which is compatible with a fast deactivation by electron transfer (Fig. 6A). The opposite effect is observed for the transient at 530 nm, *i.e.*, it's lifetime is 4 times shorter in an air-equilibrated sample than in a nitrogen purged one (Fig. 6B, τ increases from 2 to 8 μs by purging the sample with nitrogen), in agreement with the mechanism of suppression by oxygen as in reaction (4) (Scheme 3).

Because the suppression of $MB^{\bullet}$ by oxygen in air-equilibrated solution is an efficient process, it does not allow quantitative back electron transfer between the redox pair formed ($MB^{2+\bullet}$ and $MB^{\bullet}$). The spectral fingerprint of the $MB^{2+\bullet}$ species has not been published. Based on our reaction scheme (Scheme 3), $MB^{2+\bullet}$ is possibly the long-lived intermediate absorbing at 590 nm. The $MB^{2+\bullet}$ lifetime (~300 μs) is independent of the oxygen concentration and it does not react with other oxidizing molecules like methyl viologen (data not shown). Additionally, the species absorbing at 590 nm reacts with DABCO, a well-known reducing agent, suggesting that it is in an oxidized state. It can be observed that the transient at 590 nm is quenched by DABCO with a bimolecular constant of $\sim 6 \times 10^6$ M^{-1} s^{-1} (Fig. 6C). Most of the reported rates for the reaction of DABCO with triplets and radical cations are diffusion controlled ($>10^9$ M^{-1} s^{-1}) in isotropic solution.[54] For instance, the second order rate constant for the suppression of C_{60} triplets by DABCO is 2.5×10^9 M^{-1} cm^{-1} in toluene.[55] However, this same reaction is around two orders of magnitude slower in micellar solution.[55] Our results are in agreement with the smaller suppression efficiency of DABCO in micellar solution. We may speculate that these small rate constants may be due to a lower diffusion rate of DABCO in micelles. However, this effect needs to be further investigated. Therefore, when SDS is added to the MB^+ solution at the proper concentration to maximize MB^+ dimers in the micelle pseudo-phase, electron transfer processes are facilitated, forming $MB^{\bullet}$ and $MB^{2+\bullet}$ species.

This outlined photochemical pathway (Scheme 3) indicates that the production of $^1O_2$ should approach zero in the condition that the MB^+ monomer/dimer equilibrium is moved to the dimer side in the micelle pseudo-phase (Scheme 3). The light emission due to $^1O_2$ (1270 nm) was measured as a function of the SDS concentration (Fig. 7). With the increase in SDS concentration, the 1270 nm emission intensity decreases, approaching a value close to zero at a SDS concentration that maximizes dimers (Fig. 7). Above this concentration, the light emission increases following the decrease of MB^+ dimers as the micelle concentration increases. The fact that at high surfactant concentration the $^1O_2$ emission is larger than the emission observed in water can be explained by the increase in triplet yield formation observed in 50 mM SDS micelles when compared to water, as measured by triplet–triplet absorption at 420 nm, as well as by the increased oxygen concentration in the micelle pseudo-phase. [27d] This experiment shows that the efficiency of $^1O_2$ generation by MB^+ can be modulated by the presence of the right amount of SDS micelles and MB^+ species.

Conclusion

Having opposite charges, MB^+ and SDS form complexes in solution, which change the micelle and the dye properties. The alterations in the micelle and dye equilibria were monitored by surface tension and UV–VIS/fluorescence measurements, respectively. Compared with pure SDS, SDS/MB^+ complex has a higher tendency to migrate to the air/water interface and to form micelles at lower SDS concentration. An excess of MB^+ dimers in relation to monomers was observed at relatively low SDS concentration (few millimolar) and only monomers are present at high SDS concentrations (above 20–30 times the c.m.c.). The dimerization equilibria in micelle solution can be understood qualitatively by a pseudo-phase type model, which strictly considers the monomer/dimer equilibria in the micelle pseudo-phase.

The negatively charged micelle interfaces induce dimer formation of positively charged sensitizers and are able to shift a type II into a type I sensitization mechanism, practically abolishing $^1O_2$ generation. These findings are of relevance to PDT, where the sensitizer reacts in direct contact with membranes, which can vary from the slightly negative cytoplasmatic membranes to the highly negatively charged internal mitochondrial membrane without mentioning the negatively

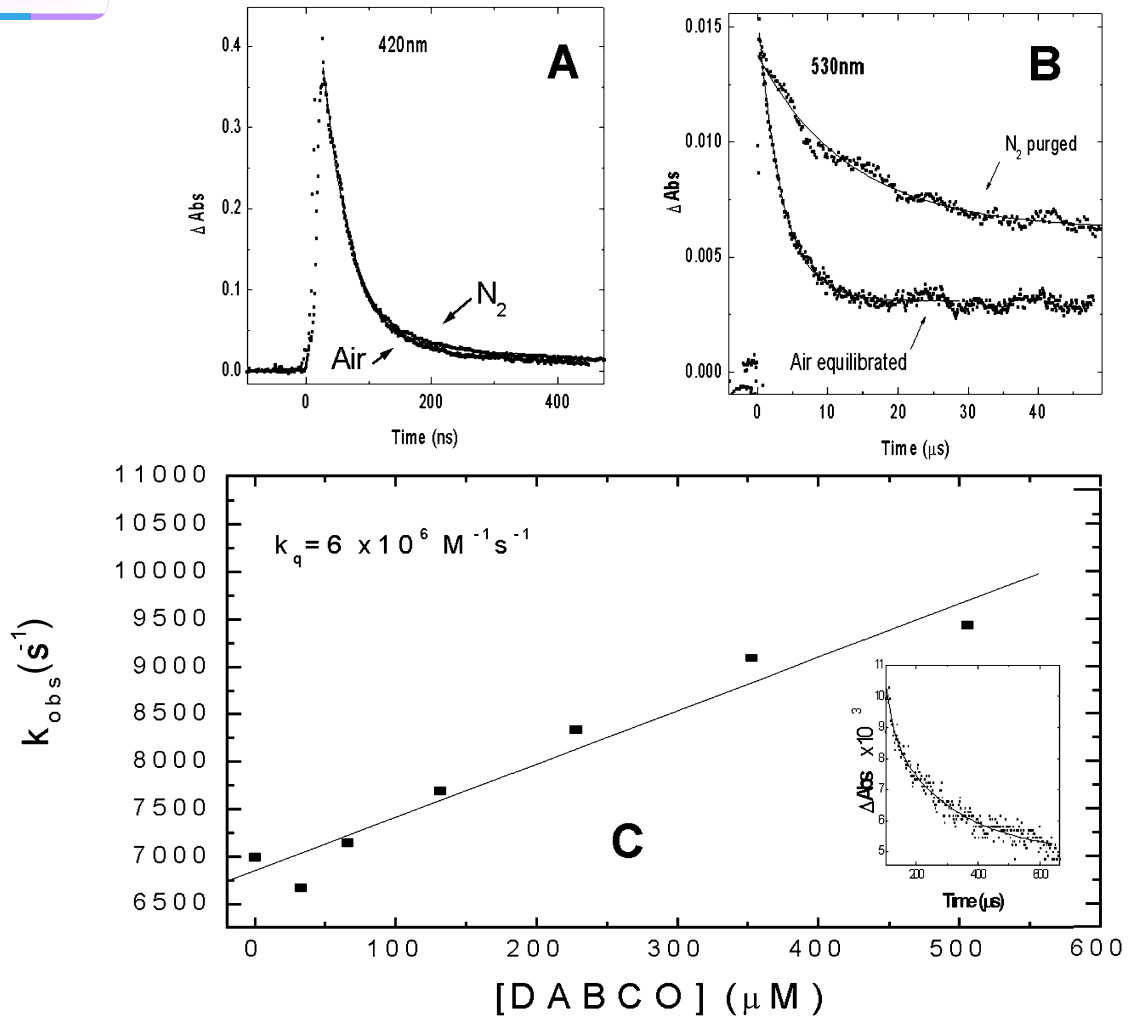

Fig. 6 Transient absorption obtained at 420 nm (A) and 530 nm (B) of MB^+/SDS solution in nitrogen-purged and air-equilibrated samples. (C) Decay rate constant of the 590 nm transient as a function of DABCO concentration. Inset: Transient decay obtained at 590 nm. $[MB^+] = 30$ μM, [SDS] = 1 mM.

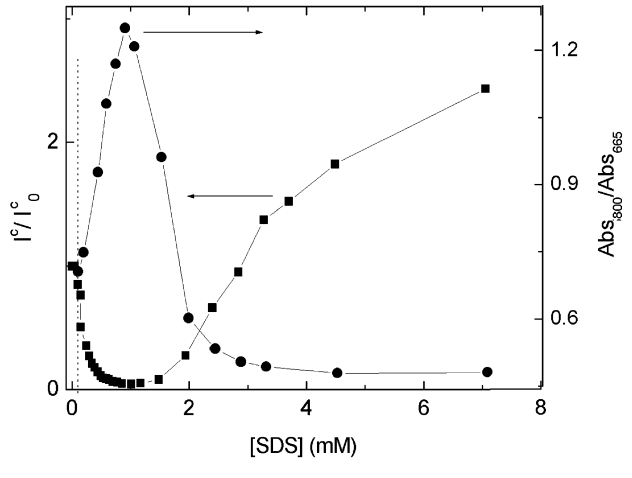

Fig. 7 Left axis: Relative change (emission at a certain SDS concentration divided by the emission without SDS, (I^C/I_0^C) in corrected NIR emission (I^C) as a function of SDS concentration. I^C is the 1270 nm emission divided by the fraction of light absorbed at 532 nm. Right axis: MB^+ absorbance at 580 nm divided by the absorbance at 665 nm as a function of SDS concentration. $[MB^+] = 30$ μM in D_2O, $\lambda_{exc} = 532$ nm, 15 mJ $pulse^{-1}$. The dashed line represents the c.m.c. of SDS at this MB^+ concentration (c.m.c. ~100 μM).

charged polyelectrolytes (DNA).[56–58] Therefore, these negatively charged interfaces can alter the mechanism and sensitization efficiency of positively charged sensitizers. This is specially important in the light of the work of Kochevar's group, which characterized that $^1O_2$ and not oxidizing radicals derived from sensitizer can induce apoptosis in cells.[59] Therefore, changing the photochemical route also shifts the mechanism and the efficiency of cell damage. Additionally, finding ways to modulate and to control the photochemistry of dyes by adsorption at charged interfaces, may also be useful for several areas of present photochemical interest, including energy conversion[60] and photography.[61]

Acknowledgements

This work has been supported by FAPESP and CNPq. H.C. Junqueira is an undergraduate fellow from the IQ-USP supported under a PIBIC program. Dr. Severino acknowledges his postdoctoral fellowship from FAPESP. D. Briotto is acknowledged for his competent technical assistance and M. J. Politi for helpful discussions.

References

1 V. Balzani and F. Scandola, in *Energy Resources Through Photochemistry and Catalysis*, ed. M.Grätzel, Academic Press, New York, 1983.
2 K. Kalyanasundaran, *Photochemistry in Microheterogeneous Systems*, Academic Press, New York, 1987.
3 B. W. Henderson and T. J. Dougherty, *Photochem. Photobiol.*, 1992, **55**, 145.
4 M. Ochsner, *J. Photochem. Photobiol. B*, 1997, **39**, 1.
5 C. S. Foote, *Science*, 1968, **162**, 963.
6 E. B. Borba, C. L. C. Amaral, M. J. Politi, R. Villalobos and M. S. Baptista, *Langmuir*, 2000, **16**, 5900.
7 W. S. L. Strauss, R. Sailer, M. H. Gschwend, H. Emmert, R. Steiner and H. Schneckenburger, *Photochem. Photobiol.*, 1998, **67**, 363.
8 (*a*) M. S. Baptista and G. L. Indig, *J. Phys. Chem. B*, 1998, **102**, 4678; (*b*) M. S. Baptista and G. L. Indig, *Chem. Commun.*, 1997, **18**, 1791.
9 (*a*) L. F. V. Ferreira, A. S. Oliveira, F. Wilkinson and D. Worral, *J. Chem. Soc., Faraday Trans.*, 1996, **92**, 1217; (*b*) G. Masci, A. Barbetta, M. Dentini and V. Crescenzi, *Macromol. Chem. Phys.*, 1999, **200**, 1157.
10 (*a*) S. C. M. Gandini, V. E. Yushmanov, I. E. Borissevitch and M. Tabak, *Langmuir*, 1999, **15**, 6233; (*b*) M. G. Neumann and M. H. Gehlen, *J. Colloid Interface Sci.*, 1990, **135**, 209.
11 T. H. James, *The Theory of the Photographic Process*, Macmillan, New York, 4th edn., 1977.
12 L. N. Guo, I. Arnaud, M. Petit-Ramel, R. Gauthier, C. Monnet, P. Leperchec and Y. Chevalier, *J. Colloid Interface Sci.*, 1994, **163**, 334.
13 E. Barni, P. Savarino and G. Viscardi, *Acc. Chem. Res.*, 1991, **24**, 98.
14 J. H. Fendler, *Membrane Mimetic Chemistry*, Wiley-Interscience, New York, 1982.
15 (*a*) M. H. Gehlen, M. Ferreira and M. G. Neumann, *J. Phochem. Photobiol. A*, 1995, **87**, 55; (*b*) M. Gratzel, *Tetrahedron*, 1987, **43**, 1679
16 J. H. Fendler, *Tetrahedron*, 1987, **43**, 1689.
17 B. E. Horsey and D. G. Whitten, *J. Am. Chem. Soc.*, 1978, **100**, 1293.
18 E. Oliveros, P. Pheulpin and A. M. Braun, *Tetrahedron*, 1987, **43**, 1713.
19 R. Sakellarioufarques, M. T. Maurette, E. Oliveros, M. Riviere and A. Lattes, *J. Photochem.*, 1982, **18**, 101.
20 R. Sakellarioufarques, M. T. Maurette, E. Oliveros, M. Riviere and A. Lattes, *Tetrahedron*, 1984, **40**, 2381.
21 E. N. Step and N. J. Turro, *J. Photochem. Photobiol. A*, 1994, **84**, 249.
22 U. Resch, S. M. Hubig and M. A. Fox, *Langmuir*, 1991, **7**, 2923.
23 M. H. Kleinman, T. Shevchenko and C. Bohne, *Photochem. Photobiol.*, 1998, **67**, 198.
24 L. A. Martínez, A. M. Braun and E. Oliveros, *J. Photochem. Photobiol. B*, 1998, **45**, 103.
25 A. Blum and L. I. Grossweiner, *Photochem. Photobiol.*, 1985, **41**, 27.
26 E. Reddi, G. Jori, M. A. J. Rodgers and J. D. Spikes, *Photochem. Photobiol.*, 1983, **38**, 639.
27 (*a*) F. Wilkinson, W. P. Helman and A. B. Ross, *J. Phys. Chem. Ref. Data*, 1995, **24**, 663; (*b*) P. B. Merkel and D. R. Kearns, *J. Am. Chem. Soc.*, 1972, **94**, 1029; (*c*) E. A. Lissi, M. V. Encinas, E. Lemp and M. A. Rubio, *Chem. Rev.*, 1993, **93**, 699.
28 M. E. Daraio, P. F. Aramendía, E. A. SanRomán and S. E. Braslavsky, *Photochem. Photobiol.*, 1991, **54**, 367.
29 J. L. Ravanat, J. Cadet, K. Araki, H. E. Toma, M. H. G. Medeiros and P. Di Mascio, *Photochem. Photobiol.*, 1998, **68**, 698.
30 J. A. Bartlett and G. L. Indig, *Photochem. Photobiol.*, 1999, **70**, 490.
31 C. Tanielian, R. Mechin, R. Seghrouchni and C. Schweitzer, *Photochem. Photobiol.*, 2000, **71**, 12.
32 R. W. Redmond and J. N. Gamlin, *Photochem. Photobiol.*, 1999, **70**, 391.
33 N. Kosui, K. Uchida and M. Koizumi, *Bull. Chem. Soc. Jpn.*, 1965, **38**, 1958.
34 D. Harmatz and G. Blauer, *Photochem. Photobiol.*, 1983, **38**, 385.
35 E. Silva, C. De Landea, A. M. Edwards and E. Lissi, *J. Photochem. Photobiol. B*, 2000, **55**, 196.
36 J. E. Schneider, T. Tabatabaie, L. Maidt, R. H. Smith, X. Nguyen, Q. Pye and R. A. Floyd, *Photochem. Photobiol.*, 1998, **67**, 350.
37 E. M. Tuite and J. M. Kelly, *J. Photochem. Photobiol. B*, 1993, **21**, 103.
38 M. Wainwright, *Chem. Soc. Rev.*, 1996, **25**, 351.
39 T. Ito and K. Kobayashi, *Photochem. Photobiol.*, 1977, **26**, 581.
40 R. Pottier, R. Bonneau and J. Joussotdubien, *Photochem. Photobiol.*, 1975, **21**, 59.
41 S. J. Wagner, A. Skripchenko, D. Robinette, J. W. Foley and L. Cincotta, *Photochem. Photobiol.*, 1998, **67**, 343.
42 A. W. Adamson and A. P. Gast, *Physical Chemistry of Surfaces*, Wiley, New York, 6th edn., 1997.
43 K. Bergmann and C. T. O'Konski, *J. Phys. Chem.*, 1963, **67**, 2169.
44 (*a*) C. Lee, Y. W. Sung and J. W. Park, *J. Phys. Chem. B*, 1999, **103**, 893; (*b*) E. Rabinomitch and L. F. Epstein, *J. Am. Chem. Soc.*, 1941, **63**, 69–78; (*c*) K. Patil, R. Pawar and P. Talap, *Phys. Chem. Chem. Phys.*, 2000, **2**, 4313.
45 (*a*) C. Tanford, *The Hydrophobic Effect: Formation of Micelles and Biological Membranes*, Wiley, New York, 1980; (*b*) P. Mukerjee and K. J. Mysels, *Critical Micelle Concentration of Aqueous Systems*, National Bureau of Standards (USA), Nat. Stand. Ref. Data. Ser., No. 36, 1970.
46 (*a*) F. H. Quina and H. Chaimovich, *J. Phys. Chem.*, 1979, **83**, 1844; (*b*) I. V. Berezin, K. Martinek and A. K. Yatsimirskii, *Russ. Chem. Rev. (Engl. Transl.)*, 1973, **42**, 787.
47 M. Nemoto, Y. Usui and M. Koizumi, *Bull. Chem. Soc. Jpn.*, 1967, **40**, 1035.
48 K. Kikuchi, H. Kokubun and M. Kikuchi, *Bull. Chem. Soc. Jpn.*, 1975, **48**, 1378.
49 S. Kato, M. Morita and M. Koizumi, *Bull. Chem. Soc. Jpn.*, 1964, **37**, 117.
50 R. M. Danziger, K. H. Bar-Eli and K. Weiss, *J. Phys. Chem.*, 1967, **71**, 2633.
51 R. Nilsson, D. R. Kearns and P. B. Merkel, *Photochem. Photobiol.*, 1972, **16**, 109.
52 L. F. Agnez-Lima, P. Di Mascio, R. L. Napolitano, R. P. Fuchs and C. F. M. Menck, *Photochem. Photobiol.*, 1999, **70**, 505.
53 R. M. Hochstrasser and M. Kasha, *Photochem. Photobiol.*, 1964, **3**, 317.
54 (*a*) M. S. Workentin, V. D. Parker, T. L. Morkin and D. D. M. Wayner, *J. Phys. Chem. A*, 1998, **102**, 6503; (*b*) B. M. Aveline, S. Matsugo and R. W. Redmond, *J. Am. Chem. Soc.*, 1997, **119**, 11 785; (*c*) M. S. Workentin, L. J. Johnston, D. D. M. Wayner and V. D. Parker, *J. Am. Chem. Soc.*, 1994, **116**, 8279; (*d*) U. Steiner, G. Winter and H. E. A. Kramer, *J. Phys. Chem.*, 1977, **81**, 1104
55 D. M. Guldi, R. E. Huie, P. Neta, H. Hungerbuhler and K. D. Asmus, *Chem. Phys. Lett.*, 1994, **223**, 511.
56 D. Voet and J. Voet, *Biochemistry*, Wiley, New York, 2nd edn., 1995.
57 D. J. Ball, Y. Luo, D. Kessel, J. Griffiths, S. B. Brown and D. I. Vernon, *J. Photochem. Photobiol. B*, 1998, **42**, 159.
58 J. Morgan, J. E. Whitaker and A. R. Oseroff, *Photochem. Photobiol.*, 1998, **67**, 155.
59 (*a*) I. E. Kochevar, M. C. Lynch, S. G. Zhyang and C. R. Lambert, *Photochem. Photobiol.*, 2000, **72**, 548–553; (*b*) C. P. Lin, M. C. Lynch and I. E. Kochevar, *Exp. Cell Res.*, 2000, **259**, 351.
60 K. Y. Law, *J. Phys. Chem.*, 1988, **92**, 4226.
61 I. R. Gould, J. R. Lenhard, A. A. Muenter, V. Godleski and S. Farid, *J. Am. Chem. Soc.*, 2000, **122**, 11 934.